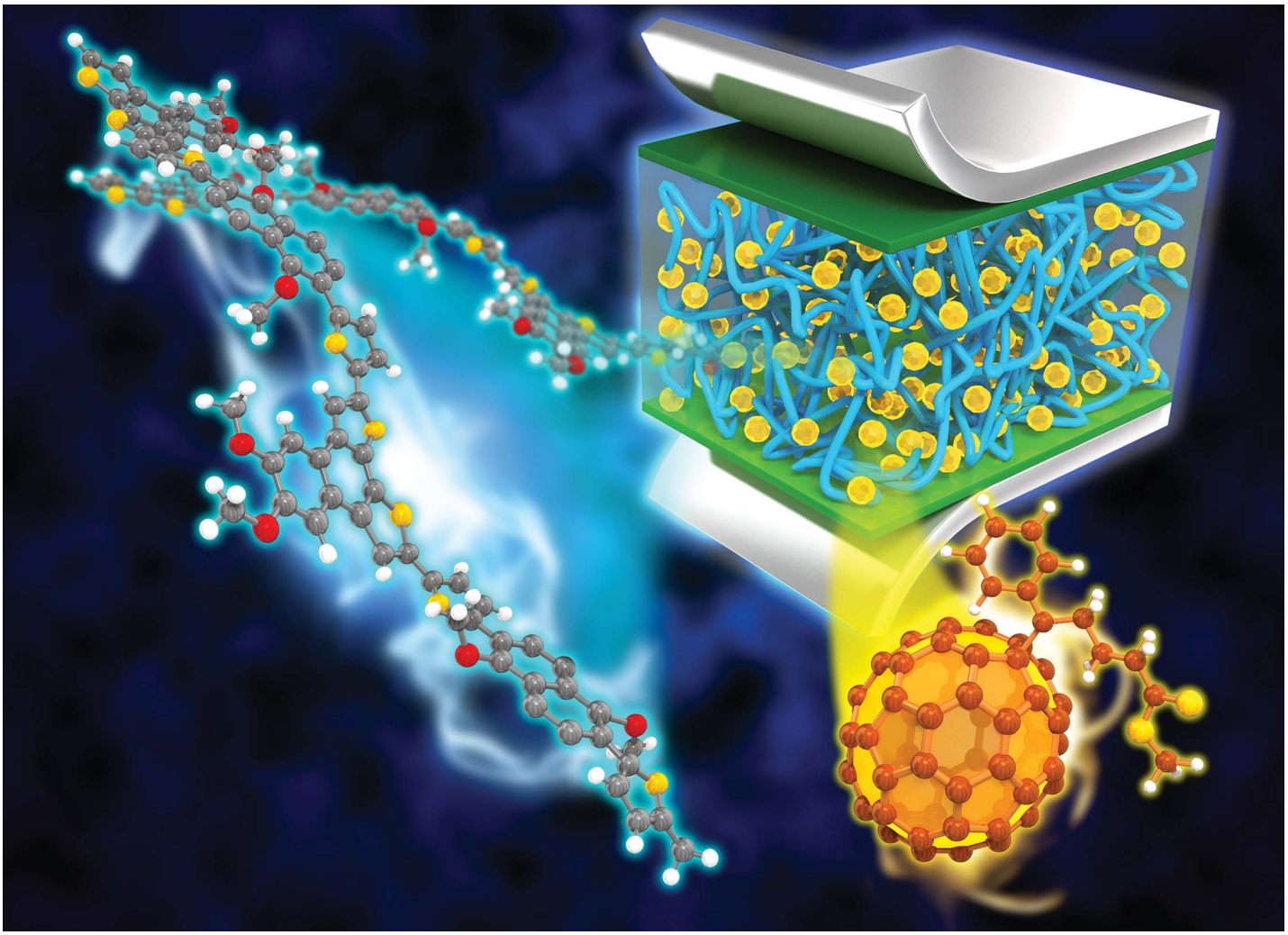

Showcasing research from Dr Chan Eon Park and colleagues at Pohang University of Science and Technology.

Title: A potential naphtho[2,1-*b*:3,4-*b*′]dithiophene-based polymer with large open circuit voltage for efficient use in organic solar cells

An efficient polymer donor material based on naphthodithiophene and alkoxy naphthalene is designed for high-performance bulk heterojunction solar cells. Using this novel polymer to effectively modify the HOMO level, resulting in significantly enhanced V_{OC}.

As featured in:

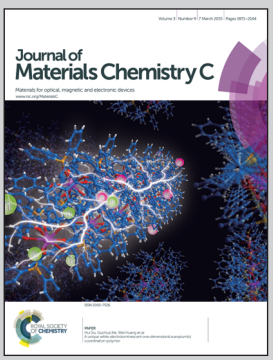

See Yun-Hi Kim, Chan Eon Park *et al.*, *J. Mater. Chem. C*, 2015, **3**, 1904.

ROYAL SOCIETY OF CHEMISTRY

www.rsc.org/MaterialsC

Registered charity number: 207890

Journal of Materials Chemistry C

PAPER

View Article Online
View Journal | View Issue

Cite this: J. Mater. Chem. C, 2015, 3, 1904

A potential naphtho[2,1-*b*:3,4-*b*′]dithiophene-based polymer with large open circuit voltage for efficient use in organic solar cells

Yu Jin Kim,[a] Ye Rim Cheon,[b] Jae-Wan Jang,[c] Yun-Hi Kim*[b] and Chan Eon Park*[a]

Received 14th November 2014
Accepted 26th December 2014

DOI: 10.1039/c4tc02597k

www.rsc.org/MaterialsC

A novel copolymer, **PNDT-BTN**, based on naphtho[2,1-*b*:3,4-*b*′]dithiophene (NDT) and alkoxy naphthalene, was designed and synthesized by the Pd-catalyzed Stille-coupling method. The copolymer demonstrated good solubility and film-forming ability, along with good thermal stability. **PNDT-BTN** exhibited a broad absorption (from 300 to 600 nm), centered at 492 nm. HOMO and LUMO energy levels of the polymer were estimated to be −5.56 eV and −3.48 eV, respectively. The polymer solar cell fabricated from the blend of the polymer (donor) and $PC_{71}BM$ (acceptor) exhibited a high power conversion efficiency of 4.29% with a high V_{OC} of 0.98 V. To the best of our knowledge, this is among the highest V_{OC} values of PSCs based on NDT derivatives. This work demonstrates that the replacement of a vinylene group in a conjugated polymer with alkoxy naphthalene moieties is able to significantly lower HOMO energy levels, and therefore, increase the open circuit voltage of solar cells.

Introduction

Bulk heterojunction (BHJ) polymer solar cells (PSCs) have attracted tremendous interest due to their potential applications in large area, lightweight, flexible photovoltaic devices through low-cost solution-processable techniques.[1–3] The power conversion efficiency (PCE) of PSCs has shown rapid improvement over the past few years. However, PCEs of polymer-based conventional single-junction BHJ cells are typically in the range of 6–8%.[4–6] Although PCEs exceeding 9% were recently achieved,[7] such high values are limited, and therefore, the development of high-performance semiconducting polymers is awaited.

Important factors to consider in the development of semiconducting polymers are: the introduction of π-cores that would ensure strong intermolecular interactions,[8–10] planar molecular structures that pack closely to form crystalline structures, enhancement of charge carrier mobility, and a large short-circuit current (J_{SC}).[11–13] Based on the above considerations, we recently reported that **PNDT-TET**, a copolymer comprising naphtho[2,1-*b*:3,4-*b*′]dithiophene (NDT) and bithiophene units coupled by vinyl groups, exhibits good photovoltaic properties with a PCE of 3.5%.[14] Although this copolymer demonstrates superior performance, one drawback of the **PNDT-TET** system is its low open circuit voltage (V_{OC}) (*i.e.*, the **PNDT-TET** device exhibits a low V_{OC} value, 0.62 V). This is likely attributable to a significant increase in the highest occupied molecular orbital (HOMO) level of the polymer due to incorporation of highly planar NDT and vinyl groups in the polymer backbone.[15–17] Importantly, a low HOMO energy level is able to improve the V_{OC}, since the V_{OC} is related to the difference between the HOMO of the electron donor material and lowest unoccupied molecular orbital (LUMO) of the electron acceptor material.[18–21] Therefore, a polymer with deep HOMO energy is an important factor for high PCEs of photovoltaic devices.

Based on the above mentioned issues, we designed and synthesized a new NDT-based polymer, poly(4,5-bis(2-octyldodecyloxy))naphtha[2,1-*b*:3,4-*b*′]dithiophene-2″,2‴-(2,5-bis(hexyloxy)naphthalene-2,6-diyl)dithiophene (**PNDT-BTN**). The alkoxy group-substituted naphthalene unit was selected to replace the vinylene moiety to reduce the HOMO level of the polymer by the twisted backbone. This polymer system was chosen in an attempt to increase the PSC performance by increasing the V_{OC} through molecular design. As expected, the **PNDT-BTN** polymer exhibited a deep HOMO energy level of −5.56 eV, and thus a high V_{OC} value (0.98 V). As a result, the device performance of **PNDT-BTN** was considerably higher than **PNDT-TET**, as a direct result of the higher V_{OC} value. To the best of our knowledge, 0.98 V is among the highest V_{OC} values for PSCs based on NDT derivatives. Therefore, our preliminary results reveal that **PNDT-BTN** polymers are promising donor materials for high-performance PSCs.

[a]*POSTECH Organic Electronics Laboratory, Department of Chemical Engineering, Pohang University of Science and Technology, Pohang, 790-784, Republic of Korea. E-mail: cep@postech.ac.kr*

[b]*Department of Chemistry & ERI, Gyeongsang National University, Jin-ju, 660-701, Republic of Korea. E-mail: ykim@gnu.ac.kr*

[c]*School of Materials Science & Engineering and Research Institute for Green Energy Convergence Technology (REGET), Gyeongsang National University, Jin-ju, 660-701, Republic of Korea*

Results and discussion

Synthesis and characterization

The structure and synthetic route for **PNDT-BTN** production are shown in Scheme 1. The polymer was obtained by the Stille coupling reaction and purified by Soxhlet extraction and precipitation. The structure of the synthesized polymer was confirmed by ^{1}H-nuclear magnetic resonance (NMR). The number-average molecular weight (M_n) of **PNDT-BTN** was determined by gel permeation chromatography (GPC) using a polystyrene standard, and determined to be 68 200 g mol^{-1}, with a polydispersity index (PDI) of 2.20. The copolymer exhibited good solubility in common chlorinated solvents, such as chloroform (CF), chlorobenzene (CB) and dichlorobenzene (DCB), owing to the introduction of the long-chain alkyl group into the NDT unit. Thermal properties of **PNDT-BTN** were investigated by thermogravimetric analysis (TGA) (Fig. 1a) and differential scanning calorimetry (DSC) (Fig. 1b). TGA showed that the decomposition temperature (T_d, at a 5% weight loss) of **PNDT-BTN** is 362 °C, and thus, the copolymer exhibits good thermal stability and is highly suitable for PSC applications.[22] No endothermic or exothermic behavior was found between 50 °C and 250 °C according to the DSC measurements, implying that **PNDT-BTN** is a sufficient amorphous polymer.[23]

Optical properties

The UV-vis absorption spectra of **PNDT-BTN** in the solution and thin-film states are shown in Fig. 2a. Absorption data are summarized in Table 1. In polymer solution, **PNDT-BTN** shows an absorption profile from 300 to 600 nm, with a maximum absorption peak (λ_{max}) at 482 nm. Compared with **PNDT-TET**, **PNDT-BTN** exhibits a slightly blue-shifted absorption maximum and narrower spectrum due to incorporation of the alkoxy naphthalene unit in the polymer, which damages the coplanarity of the main chains.[24] In the thin film state, **PNDT-BTN** exhibits λ_{max} = 492 nm, approximately 10 nm red-shifted from that of the solution state. Furthermore, the longer wavelength region of the absorption peak at λ_{max} = 527 nm appears sharply, and the absorption band is broadened, indicating a stronger interchain interaction in the solid state.[25] The optical bandgap calculated from the film absorption edge was 2.12 eV.

PL spectra of the polymer and polymer blended with $PC_{71}BM$ were examined for the charge transfer process from the polymer to PCBM. Fig. 2b compares the PL spectra of **PNDT-BTN** and the **PNDT-BTN** : $PC_{71}BM$ composite in solid thin-film states with varying weight ratios (1 : 1, 1 : 2, 1 : 3, and 1 : 4). **PNDT-BTN** showed a strong PL emission band with emission maxima at approximately 600 nm, whereas the emission band for **PNDT-BTN** : $PC_{71}BM$ was nearly quenched. Moreover, as the amount of $PC_{71}BM$ increased, the **PNDT-BTN** : $PC_{71}BM$ blend exhibited a much lower quenching efficiency, suggesting that polymer excitons can efficiently diffuse into the donor–acceptor interface and dissociate into carriers.[26,27]

Electrochemical properties

Electrochemical properties of the **PNDT-BTN** polymer were measured by cyclic voltammetry (CV) to determine HOMO and LUMO energy levels. CV was performed using an electrochemical analyzer at a sweep rate of 50 mV s^{-1}. Voltage was calibrated with ferrocene oxidation potential (Fc/Fc^+). Fig. 3a shows the oxidation and reduction curves of the polymer. The oxidation and reduction onset potentials of **PNDT-BTN** were 1.21 V and −0.83 V, respectively. Table 1 summarizes the HOMO and LUMO levels; those of **PNDT-BTN** were −5.56 and −3.48 eV, respectively. Ferrocene oxidation was assumed to be 4.8 eV below the vacuum level.[28] Therefore, introduction of alkoxy naphthalene in the NDT-based polymer chain resulted in a greater impact on HOMO energy levels. The HOMO energy levels obtained electrochemically were deeper than those reported previously for an analogous NDT-based copolymer,[9,29] likely due to the introduction of alkoxy naphthalene, which increased the steric hindrance and reduced the coplanarity of

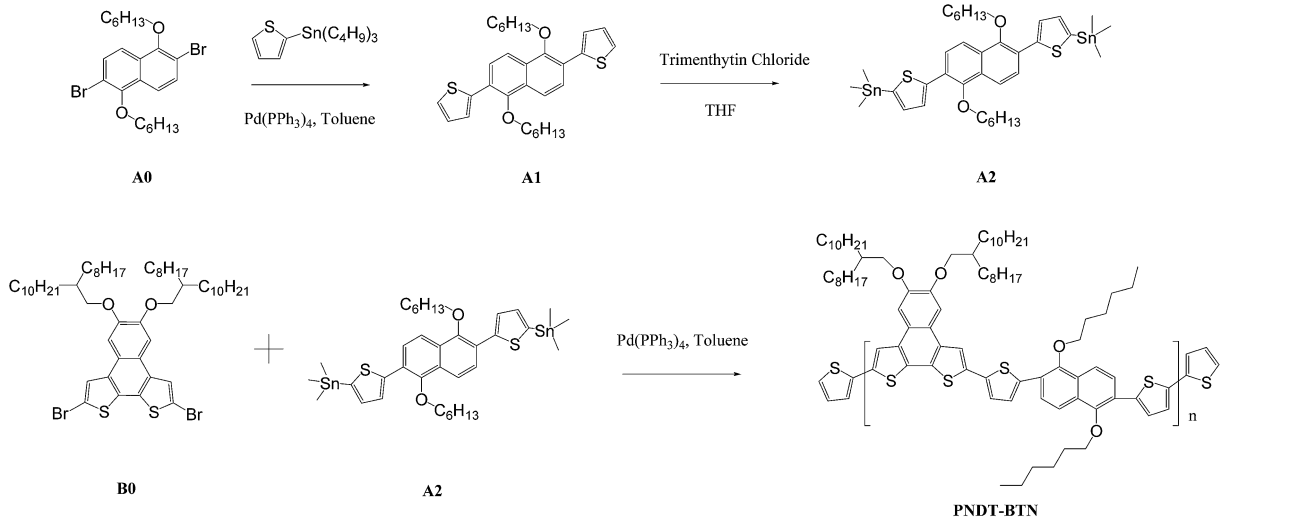

Scheme 1 Synthetic route of copolymer production.

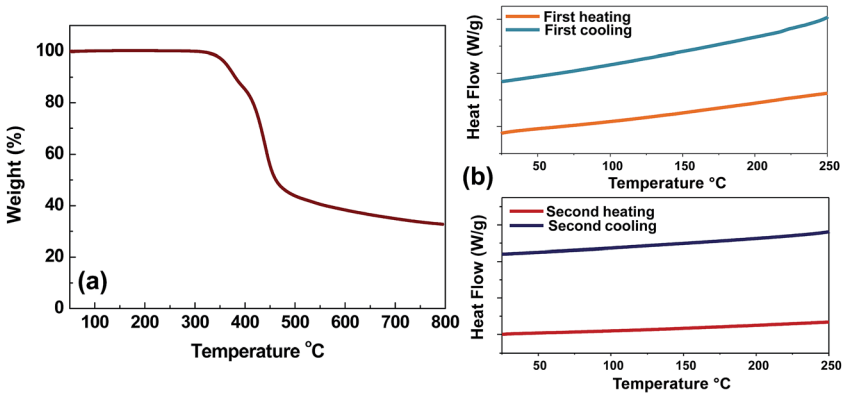

Fig. 1 TGA plot (a) and DSC trace (b) of **PNDT-BTN** at a heating rate of 10 °C min^{-1} under an inert atmosphere.

the resulting copolymers, thus leading to a reduction in HOMO orbital overlap and deeper HOMO levels.[30] This low-lying HOMO energy level of the copolymer is beneficial to the stability of the polymer against oxidation,[31] as well as a higher open-circuit voltage of the PSCs based on the polymer as donors[32] (because V_{OC} is linearly correlated with the difference between the HOMO of the donor and the LUMO of the acceptor, as described above).

Density functional theory (DFT) calculation

To further investigate the impact of alkoxy naphthalene on the optoelectronic properties of the **PNDT-BTN** copolymer, theoretical calculations were determined to reveal the HOMO and LUMO energy levels by density functional theory (DFT). Becke's three parameter gradient corrected functional (B3LYP) with a polarized 6-31 G** basis was used for full geometry optimization. To reduce the computation time, methyl alkyl groups were used to replace the long alkyl groups. HOMO and LUMO surface plots of the ground-state optimized structures are illustrated in Fig. 3b. The HOMO is located predominantly on the NDT unit, whereas the LUMO contains the entire length of the backbone. The calculated HOMO and LUMO energies of the **PNDT-BTN** were −6.97 eV and −4.95 eV, respectively, and the band gap was determined to be 2.02 eV. The calculated values of the ground HOMO, LUMO and band gap are in agreement with values obtained from the electrochemical and optical measurements from **PNDT-BTN**.

Structural electronic properties of the conjugated polymer were also investigated. Fig. 4 shows the geometry optimization of **PNDT-BTN** oligomers at the ground state, and the related data from **PNDT-TET** were evaluated for comparison. The results revealed that **PNDT-BTN** has a fairly twisted backbone, indicating that this polymer has higher rotational disorder.[33] In contrast, the **PNDT-TET** oligomer with two covalently fastened thiophene spacers to the vinylene group resulted in a highly planar conformation with torsion angles of <0.6°. These findings indicate that the **PNDT-BTN** polymer has a more amorphous characteristic than **PNDT-TET**, consistent with DSC analysis.[34,35]

Hole carrier mobility

In order to confirm the influence of molecular structures on the charge carrier hole mobilities of copolymers, hole mobilities of **PNDT-BTN** and **PNDT-TET** were measured using organic field-effect transistor (OFET) and SCLC techniques. As depicted in Fig. 5, the typical transfer and output curves were generated by the OFET method. Both devices exhibited a moderate p-type organic semiconductor behavior, as well as good linear and

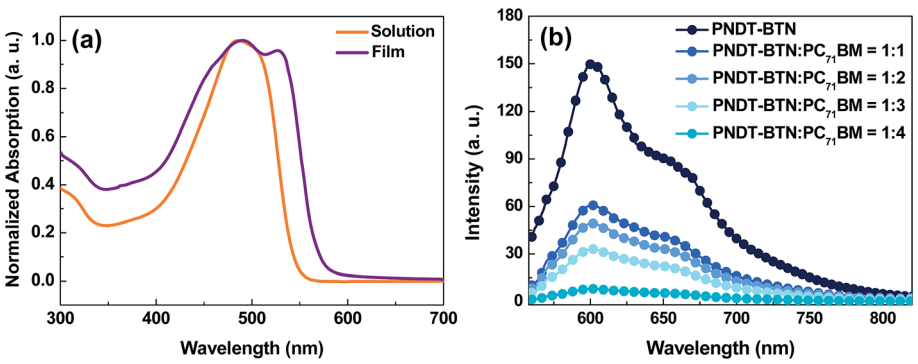

Fig. 2 Normalized absorption spectra of **PNDT-BTN** in chloroform solution, and solid-film (a) and photoluminescence (PL) spectra of the pristine polymer and polymer:$PC_{71}BM$ blended film (b).

Table 1 Optical and electrochemical properties of the PNDT-BTN polymer

	UV-vis absorption spectrum				Cyclic voltammetry			
Polymer	λ_{max} (nm) solution	λ_{max} (nm) film	λ_{onset} (nm) film	E_g^{opt} (eV)[a]	E_{onset}^{ox} (eV)	E_{onset}^{red} (eV)	E_{HOMO} (eV)	E_{LUMO} (eV)
PNDT-BTN	482	492, 527	584	2.12	1.21	−0.83	−5.56	−3.48

[a] Estimated from the absorption edge in film ($E_g^{opt} = 1240/\lambda_{onset}$ eV).

saturation characteristics. The average hole mobilities of **PNDT-BTN** and **PNDT-TET** among five devices were 3.2×10^{-3} cm^2 V^{-1} s^{-1} and 2.6×10^{-2} cm^2 V^{-1} s^{-1}, respectively. The difference is far more than an order of magnitude, indicating that **PNDT-BTN** undergoes fewer intermolecular interactions than **PNDT-TET**.[36] On the basis of these OFET mobility results, we conclude that the **PNDT-BTN** polymer has more amorphous regions than **PNDT-TET**, inducing less intermolecular packing and thus reducing mobility.

The hole mobilities of **PNDT-BTN** and **PNDT-TET** were also measured using the SCLC model, which uses a device structure of ITO/PEDOT : PSS/**PNDT-BTN** or **PNDT-TET** : $PC_{71}BM$/Au. Experimental details are described in the 'Experimental' section. Results are plotted in Fig. 5. Hole mobilities of **PNDT-BTN** and **PNDT-TET** were calculated to be 5.62×10^{-4} cm^2 V^{-1} s^{-1} and 4.92×10^{-3} cm^2 V^{-1} s^{-1}, respectively (Fig. 5c and f). **PNDT-BTN** also showed a slightly reduced mobility compared with that of its analogue, **PNDT-TET**; this slightly reduced mobility likely originated from the region-random structure of the **PNDT-BTN** polymer, consistent with DFT analysis.[37,38]

Photovoltaic response

To explore the solar cell properties of **PNDT-BTN**, conventional BHJ PSCs were fabricated and evaluated according to our previous work. The device structure used was ITO/PEDOT : PSS/**PNDT-BTN** : $PC_{71}BM$/LiF/Al. $PC_{71}BM$ was chosen instead of $PC_{61}BM$ due to its significantly broader and stronger absorption in the visible region.[39] All PSC devices in this work were evaluated under simulated 100 mW cm^{-2}, AM 1.5G illumination. The current density–voltage (J–V) curves are plotted in Fig. 6a, and the photovoltaic data of open circuit voltage (V_{OC}), short circuit current (J_{SC}), fill factor (FF) and PCE are summarized in Table 2. The blend ratio was an important factor that influenced the device performance; therefore, we carefully tuned the blend ratio of the active layers between a ratio of 1 : 1 and 1 : 4 (w/w), polymer : $PC_{71}BM$, in a dichlorobenzene (o-DCB) solution. A weight ratio of 1 : 4 (w/w) for the active layers displayed the best performance for the **PNDT-BTN** : $PC_{71}BM$ devices, with a high PCE of 4.29%, a V_{OC} of 0.98 V, a J_{SC} of 8.7 mA cm^{-2}, and a FF of 50.3%. According to photovoltaic measurements, with increasing PCBM weight ratio, J_{SC} and FF showed a trend towards a gradual increase; one possible explanation for this phenomenon may be from a relatively percolated homogeneous film with smaller roughness, as described in the 'Morphology' section. Interestingly, compared with the **PNDT-TET** device, the PSC performance of **PNDT-BTN** was much higher, as shown in Table 2, particularly the V_{OC}, which could be due to the deeper HOMO energy level. This is in good agreement with our synthesis strategy and results from the CV study, in which **PNDT-BTN** exhibited a significantly lower HOMO level than **PNDT-TET**.

To verify the PCE of these devices, we investigated EQE spectra based on the **PNDT-BTN** : $PC_{71}BM$ blend as an active layer with varying weight ratios (Fig. 4b). The EQE curves show a broad wavelength range of 300–600 nm. Increasing concentrations of PCBM resulted in a higher and broader coverage of EQE, leading to a considerable increase in J_{SC}.[40] This observation is in agreement with J–V characteristics. In particular, the **PNDT-BTN** : $PC_{71}BM$ with 1 : 4 w/w exhibited a maximum EQE of ~48% at 503 nm, whereas the **PNDT-BTN** : $PC_{71}BM$ with 1 : 1 w/w showed a maximum EQE of ~34% at 502 nm. These results support the 1.4-fold higher photocurrent value in the

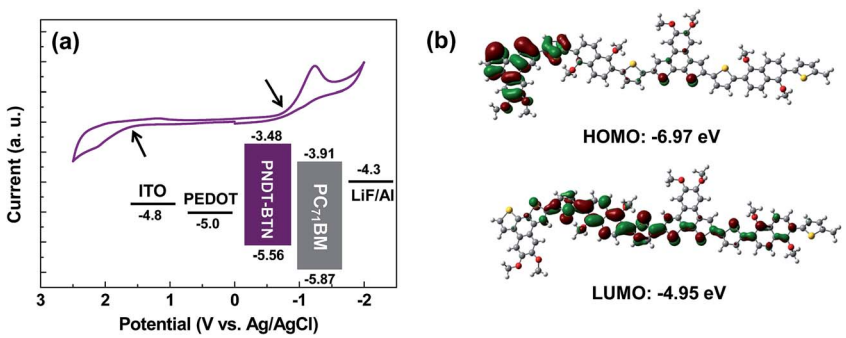

Fig. 3 Cyclic voltammograms of PNDT-BTN (inset, energy levels of a PNDT-BTN-based single junction device) (a) and HOMO/LUMO wave functions of the oligomers of PNDT-BTN (b).

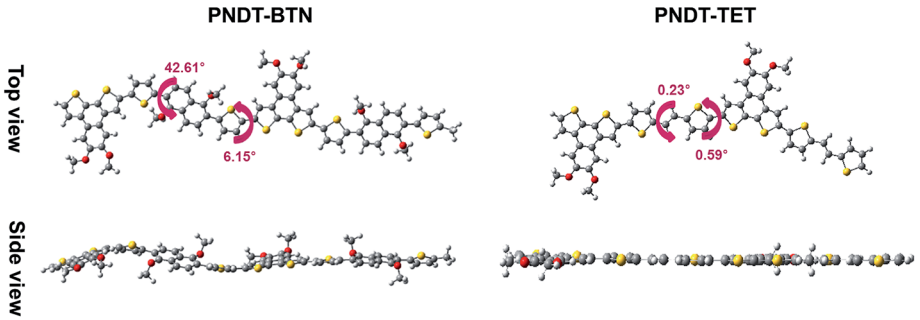

Fig. 4 Molecular geometries of PNDT-BTN and PNDT-TET dimers.

PNDT-BTN : $PC_{71}BM$ (1 : 4, w/w) device compared with the **PTPD-BTN** : $PC_{71}BM$ (1 : 1, w/w) cell.[41]

Morphological properties

A suitable morphology is beneficial not only for exciton separation but also for charge transfer to respective electrodes and charge collection. Atomic force microscopy (AFM) was utilized to investigate the surface morphology of **PNDT-BTN** : $PC_{71}BM$ (1 : 1, 1 : 2, 1 : 3, and 1 : 4 w/w) blend films spin-coated from an *o*-DCB solution. The resulting height and phase images are shown in Fig. 7. The connectivity was sensitive to the blend ratio of **PNDT-BTN** to $PC_{71}BM$. As the amount of $PC_{71}BM$ increased, the nanoscale percolated network and reduced phase separation became more apparent, with gradual emergence of a 'fibrillar' **PNDT-BTN** nanostructure. This fibrillar **PNDT-BTN** nanostructure was most pronounced in films at the 1 : 4 blend ratio, implying that increasing amounts of $PC_{71}BM$ cause the **PNDT-BTN** network to form longer and better-connected pathways, which may explain the higher J_{SC} and FF values.[42–44] These results are also in agreement with the results of the above PL quenching data. Because the PL quenching efficiency can directly reflect the polymer domain size in blend, the 1 : 4 w/w PNDT-BTN : $PC_{71}BM$ film with the smallest domain size exhibited the lowest quenching efficiency (see Fig. 2b). In addition, root mean-square roughness (rms) values for the blend films gradually decreased to 5.38, 4.01, 2.23, and 1.57 nm at ratios of 1 : 1, 1 : 2, 1 : 3, and 1 : 4, respectively. This result is consistent with previous reports in which smoother blend films displayed better performance in BHJ solar cells.[45,46] Specifically, relating the AFM images to the device data suggests that an increasing amount of $PC_{71}BM$ in the active layer produces a better bi-continuous network, inducing efficient exciton dissociation, and thus leading to an increase in the photocurrent density and FF, as well as device efficiency.[47]

Nanostructure order

To obtain information regarding the molecular packing in the pristine films and blend films with $PC_{71}BM$, the XRD patterns of the pure polymer and blend films were measured (Fig. 8a and b). The results for the pure **PNDT-BTN** film showed no

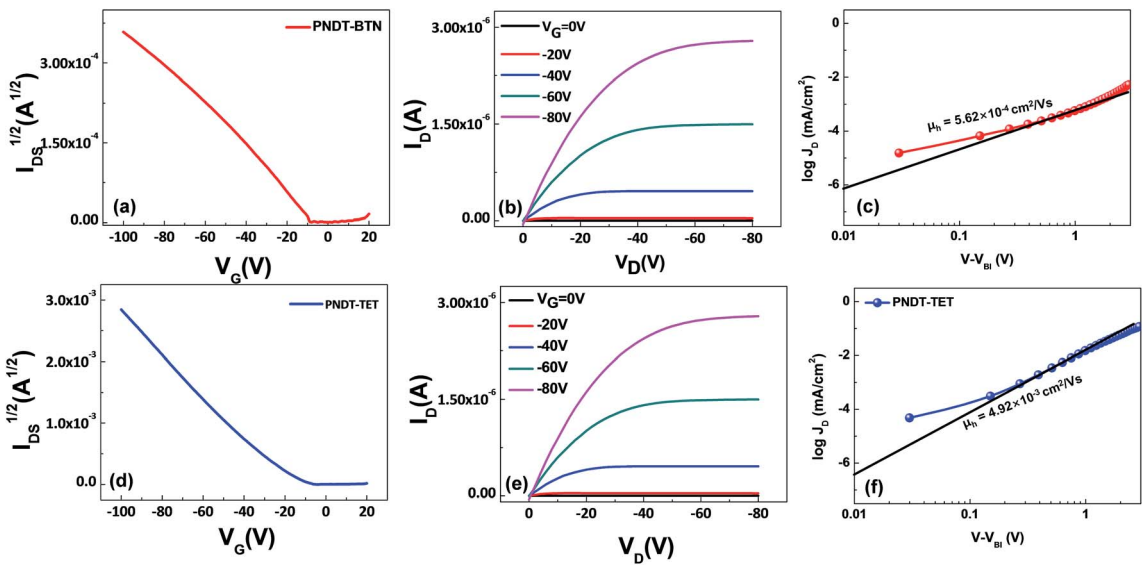

Fig. 5 Transfer characteristics of both polymers, measured at $V_{ds} = -80$ V (a and d). Output characteristics with V_{DS} varying from 0 V to −80 V (at 10 V increments) deposited onto ODTS-modified SiO_2 (b and e). *J*–*V* curves of **PNDT-BTN** and **PNDT-TET** films for hole mobility by the SCLC method (c and f) (upper panel, **PNDT-BTN**; lower panel, **PNDT-TET**).

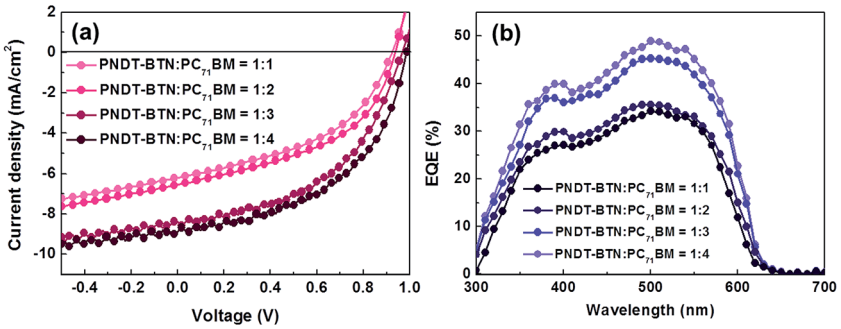

Fig. 6 *J*–*V* characteristics of BHJ photovoltaic devices based on **PNDT-BTN** : $PC_{71}BM$ (a). EQE spectra of PSCs based on **PNDT-BTN** and $PC_{71}BM$ (b).

Table 2 Performance parameters of polymer solar cells using $PC_{71}BM$ as an electron acceptor (varying weight ratios, w/w)

Polymer	Blend ratio	V_{OC} (V)	J_{SC} (mA cm^{-2})	FF (%)	PCE (%)
PNDT-BTN	1 : 1	0.92	6.2	45.7	2.61
	1 : 2	0.94	6.5	47.2	3.00
	1 : 3	0.97	8.4	49.5	4.03
	1 : 4	0.98	8.7	50.3	4.29
PNDT-TET[13]	1 : 2	0.62	9.1	62.6	3.50

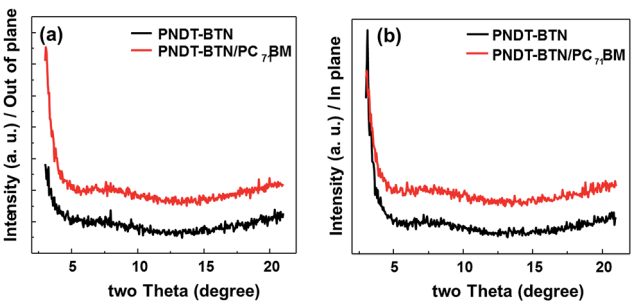

Fig. 8 Out-of-plane and in-plane XRD patterns of pure **PNDT-BTN** (black line) and **PNDT-BTN** : $PC_{71}BM$ blended films (1 : 4 w/w, red line).

crystalline diffraction peaks in either the out-of-plane or in-plane directions, indicating that the **PNDT-BTN** polymer contains more amorphous regions than do crystalline planes.[48] This result also demonstrates that, in agreement with our synthesis strategy, incorporation of the alkoxy naphthalene unit in NDT-based polymers results in a polymer with an amorphous structure, consistent with DSC, DFT and hole mobility analyses.

Likewise, the diffraction patterns of **PNDT-BTN** : $PC_{71}BM$ blend films were similar to those of the pure polymer films. Moreover, the **PNDT-BTN** blend produced no diffraction peaks, suggesting that the **PNDT-BTN** blend contains small domains of homogeneously blended PNDT-BTN and $PC_{71}BM$ components, which is in agreement with the results of our AFM study.[49,50]

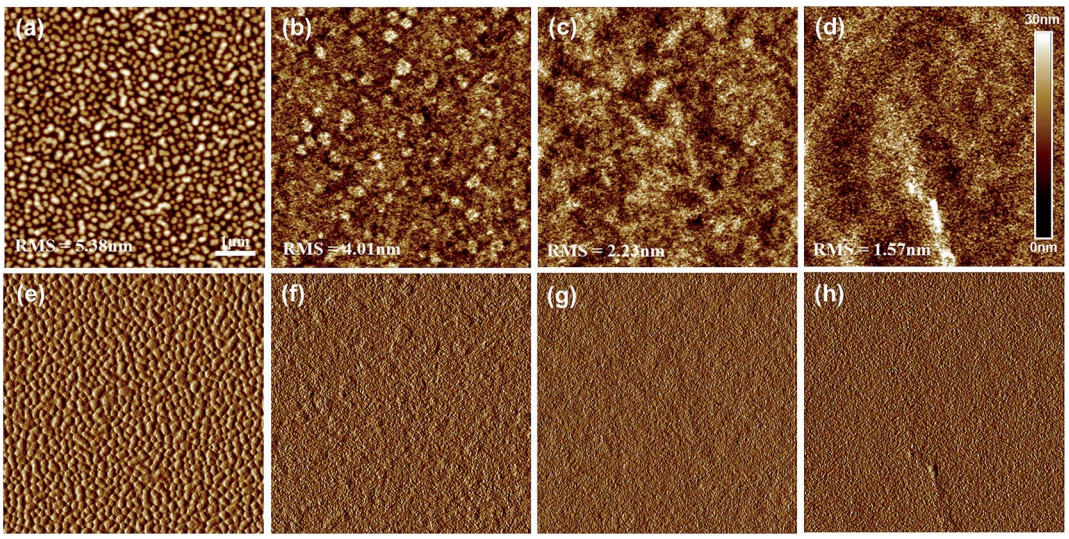

Fig. 7 AFM height and phase images for **PNDT-BTN** : $PC_{71}BM$ blend films with different weight ratios spin-coated from *o*-DCB at the following ratios: 1 : 1 (a and e), 1 : 2 (b and f), 1 : 3 (c and g), and 1 : 4 (d and h).

Conclusions

We designed and synthesized a novel NDT-based copolymer, **PNDT-BTN**. The polymer demonstrated good thermal stability ($T_d \sim 362$ °C), good solubility in common organic solvents, and a deep HOMO energy level (−5.56 eV). The polymer solar cell fabricated from the blend of **PNDT-BTN** : $PC_{71}BM$ exhibited a high PCE of 4.29% with a high V_{OC} of 0.98 V, which benefitted from the low HOMO level of the polymer. These results demonstrate the potential of the replacement of the vinylene group with alkoxy naphthalene units in the design and synthesis of conjugated polymers with efficient solar cell performance, and that the resulting lower HOMO energy levels of conjugated polymers increase the open circuit voltage of solar cells. Most importantly, this work opens up a new method of designing high-performance photovoltaic materials.

Experimental section

Materials

All chemical reagents were purchased from Sigma-Aldrich and used as directed. 2,6-Dibromo-1,5-bis(hexyloxy)naphthalene (**A0**) and 2,9-dibromo-4,5-bis(2-octyldodecyloxy)naphtho[2,1-*b*:3,4-*b*′]dithiophene (**B0**) were prepared according to literature procedures.[51–53] Additional materials were of common commercial grade and used as directed. All solvents were further purified prior to use.

Synthesis of PNDT-BTN

2,2′-(1,5-Bis(hexyloxy)naphthalene-2,6-diyl)dithiophene (A1). 2,6-Dibromo-1,5-bis(hexyloxy)naphthalene (**A0**) (3.0 g, 6.5 mmol) was dissolved in toluene (50 mL). Trimethyl(thiophen-2-yl)stannane (5.3 g, 14.3 mmol) and $Pd(PPh_3)_4$ (0.6 g, 0.52 mmol) were added to the mixture. The mixture was then refluxed for 12 h at 90 °C. After cooling to room temperature, the mixture was quenched with water, extracted with ethyl acetate and desiccated with $MgSO_4$. The product was purified by chromatography using hexane. Yield: 2.3 g, 4.7 mmol (78%). ^{1}H-NMR (300 MHz, $CDCl_3$): δ 7.97 (92H, d), 7.82 (92H, d), 7.63 (2H, d), 7.44 (2H, d), 7.17 (2H, t), 3.90 (4H, t), 2.01–1.92 (4H, m), 1.57–1.51 (4H, m), 1.42–1.36 (8H, m), 0.95 (6H, t). ^{13}C-NMR (300 MHz, $CDCl_3$): δ 151.42, 139.43, 129.56, 126.97, 126.82, 126.27, 125.79, 123.46, 118.93, 87.57, 74.23, 31.74, 30.39, 25.74, 22.64, 14.07. High-resolution mass spectrometry (HRMS) (EI+) *m*/*z* calculated for $C_{30}H_{36}O_2S_2$ = 492.2157; found = 492.2159.

(5,5′-(1,5-Bis(hexyloxy)naphthalene-2,6-diyl)bis(thiophene-5,2-diyl))bis(trimethylstannane) (A2). 2,2′-(1,5-Bis(hexyloxy)-naphthalene-2,6-diyl)dithiophene (**A1**) (2.2 g, 4.5 mmol) was added to a flask of THF (50 mL). *n*-BuLi (2.5 M, 4.0 mL, 9.8 mmol) was added dropwise at room temperature and stirred at 40 °C for 2 h. The mixture was cooled to 0 °C and added to trimenthytin chloride (2.13 g, 10.7 mmol). After 2 h agitation at room temperature, the mixture was quenched with ice water, extracted with ether and desiccated with $MgSO_4$. The product was purified by chromatography with aluminum oxide. Yield: 2.54 g, 3.1 mmol (70%). ^{1}H-NMR (300 MHz, $CDCl_3$): δ 7.96 (2H, d), 7.81(2H, d), 7.75 (2H, d), 7.26 (2H, d), 3.90 (4H, t), 2.01–1.92 (4H, m), 1.59–1.51 (4H, m), 1.41–1.36 (8H, m), 0.95 (6H, t), 0.44 (18H, s). ^{13}C-NMR (300 MHz, $CDCl_3$): δ 151.26, 145.33, 138.83, 129.54, 126.94, 123.50, 118.87, 74.13, 31.78, 30.41, 25.79, 22.62, 14.09, −8.24.

Poly(2-(5-(1,5-bis(hexyloxy)-6-(5-methylthiophen-2-yl)naphthalen-2-yl)thiophen-2-yl)-9-methyl-5,6-bis((2-octyldodecyl)oxy)-naphtho[2,1-*b*:3,4-*b*′]dithiophene) (PNDT-BTN). (5,5′-(1,5-Bis(hexyloxy)naphthalene-2,6-diyl)bis(thiophene-5,2-diyl))bis-(trimethylstannane) (**A2**) (1.25 g, 1.5 mmol), 2,9-dibromo-4,5-bis((2-octyldodecyloxy))naphtho[2,1-*b*:3,4-*b*′]dithiophene (**B0**) (1.5 g, 1.5 mmol), and $Pd(PPh_3)_4$ (0.12 g, 0.11 mmol) were added to a flask of toluene (60 mL). The mixture was refluxed for 48 h at 90 °C. Afterwards, 2-bromonaphthalene (0.07 g, 0.45 mmol) and trimethyl(thiophen-2-yl)stannane (0.12 g, 0.45 mmol) were added to the reaction mixture every 6 h for end-capping. The reaction mixture was cooled to room temperature and poured into 500 mL of methanol. The precipitate was collected by filtration, and the polymer was purified by successive Soxhlet extractions with acetone, hexane, and toluene. The solution was concentrated and dropped into 500 mL of methanol, and the precipitate was collected by filtration. Yield: 1.83 g (91%). ^{1}H-NMR (500 MHz, $CDCl_3$): δ 7.78 (8H, br), 7.09 (4H, br), 4.02 (8H, br), 2.01 (6H, b), 1.34 (76H, br), 0.84 (18H, br).

Chemical characterization

^{1}H-NMR spectra were recorded using a Bruker Advance-300 spectrometer and DRX-500 MHz spectrometer. HRMS (EI) spectra were collected using a high-resolution gas chromatography (GC) mass spectrometer with a LabRAM HR800 UV. Mass spectra were determined using a high-resolution 4800 Tof/Tof mass spectrometer with a Voyager DE-STR. Molecular weights and polydispersities of the copolymer were determined by gel-permeation chromatography (GPC) using a polystyrene standard. GPC was conducted using water as the mobile phase in a high-pressure GPC assembly using a Model M515 pump with u-Styragel columns of HR4, HR4E, and HR5E, which yielded 500 and 100 Å resolutions. Thermal gravimetric analysis (TGA) was performed on a TA TGA 2100 thermogravimetric analyzer under purified nitrogen at a heating rate of 10 °C min^{-1}. Differential scanning calorimetry (DSC) was conducted under nitrogen on a TA Instrument 2100 DSC. Samples were heated to 10 °C min^{-1} from 50 °C to 250 °C. The UV-Vis absorption spectra were determined using a Cary 5000 UV-vis-near-IR double beam spectrophotometer. Cyclic voltammetry (CV) was performed using a PowerLab/AD instrument model system in a 0.1 M tetrabutylammonium hexafluorophosphate (Bu_4NPF_6) solution in anhydrous acetonitrile as the supporting electrolyte, at a scan rate of 50 mV s^{-1}. A glassy carbon disk (~0.05 cm^2) coated with a thin polymer film, an Ag/AgCl electrode and a platinum wire were used as the working electrode, reference electrode and counter electrode, respectively. Density functional theory (DFT) calculations were carried out at the B3LYP/6-31G* level of theory using the Spartan 08 computational programs. An atomic force microscope (AFM) (Multimode IIIa, Digital Instruments) was operated in tapping mode to obtain surface images (surface

area: 5 × 5 μm^2) of the polymer:$PC_{71}BM$ blend films with varying blend ratios under ambient conditions. X-ray diffraction (XRD) spectra were collected at the 5A beamline (wavelength = 1.071 Å) at the Pohang Accelerator Laboratory (PAL) in Korea. Pure **PNDT-BTN** and **PNDT-BTN** : $PC_{71}BM$ blend films were prepared on a Si/PEDOT : PSS substrate using the spin-coating method.

OFET fabrication and measurement

Top-contact organic field-effect transistors (OFETs), composed of **PNDT-BTN** and **PNDT-TET**, were fabricated on a common gate of highly n-doped silicon with a 300 nm thick, thermally grown SiO_2 dielectric layer. Before substrates were modified with octadecyltrichlorosilane (ODTS), piranha solution was used to clean organic residues of silicon substrates, and surfaces were ozone-treated for 20 min. Cleaned substrates were modified with ODTS from a toluene solution for 60 min at room temperature, and films of semiconducting materials were spin-coated at 4000 rpm from 0.2 wt% chloroform solution, with a thickness of 50 nm. Gold source and drain electrodes of OFETs based on **PNDT-BTN** and **PNDT-TET** were evaporated on top of the semiconductor layers (80 nm). Channel lengths of 50 μm and channel widths of 2000 μm were used for all measurements. Electrical characteristics of the OFETs were measured in air using both Keithley 2400 and 236 source/measure units.

Hole-only device fabrication and measurement

Hole-only devices were fabricated by the configuration of ITO/PEDOT : PSS/**PNDT-BTN** or **PNDT-TET**/Au. The Au layer was deposited under a low speed (1 Å s^{-1}) to avoid penetration of Au atoms into the active layer. The device characteristics were extracted by modeling the dark current under an applied forward bias. Hole mobilities were determined by fitting the current–voltage curves with the Mott-Curney law (SCLC):

$$J = \frac{9}{8}\varepsilon_0\varepsilon_r\mu_h\frac{V^2}{L^3},$$

where J represents the current density, L represents the film thickness of the active layer, μ_h represents the hole mobility, ε_r represents the relative dielectric constant of the transport medium, ε_0 represents the permittivity of free space, V represents the internal voltage in the device, and $V = V_{appl} - V_r - V_{bi}$, where V_{appl} represents the voltage applied to the device, V_r represents the voltage drop due to contact resistance and series resistance across the electrodes, and V_{bi} represents the built-in voltage due to the relative work function difference between the two electrodes. V_{bi} can be determined from the transition between the ohmic and SCLC regions.

OPV fabrication and measurement

Devices were fabricated with the conventional structure glass/ITO/PEDOT : PSS/active layer (**PNDT-BTN** : $PC_{71}BM$)/LiF/Al using a solution process. ITO-coated glass substrates were cleaned by ultrasonic treatment in detergent, deionized water, acetone, and isopropyl alcohol under ultrasonication for 20 min each, followed by drying under a nitrogen stream. A thin layer (~40 nm) of PEDOT : PSS (Clevios P VP AI 4083, filtered at 0.45 μm PVDF) was spin-coated at 4000 rpm onto each ITO surface. After baking at 120 °C for 20 min, substrates were transferred into a nitrogen-filled glove box. A photoactive layer was subsequently spin-coated at 1000 rpm for 60 s onto each PEDOT : PSS layer. The active layer spin-coating solution was stirred in a glove box under a nitrogen atmosphere for 12 h prior to spin-coating and prepared from copolymer : $PC_{71}BM$ mixtures with weight ratios varying from 1 : 1 to 1 : 4 in 1,2-dichlorobenzene at a total concentration of 40 mg mL^{-1}. The layer thickness was approximately 100 nm. Finally, a 0.8 nm LiF layer and an 80 nm Al layer were deposited onto each active layer under high vacuum (2×10^{-6} torr). The effective area of the cells was 9 mm^2, as defined by the mask. The current density–voltage (J–V) characteristics of the photovoltaic devices were measured under ambient conditions using a Keithley Model 2400 source measurement unit. An Oriel xenon lamp (450 W) with an AM1.5G filter served as the solar simulator. The light intensity was calibrated to 100 mW cm^{-2} using a silicon cell with a KG5 filter calibrated by the National Renewable Energy Laboratory (LREL). EQE spectra were obtained from a photomodulation spectroscopic setup (model Merlin, Oriel), a calibrated Si UV detector, and a SR570 low-noise current amplifier.

Acknowledgements

This study was supported by a grant (2011-0031639) from the Center for Advanced Soft Electronics under the Global Frontier Research Program of the Ministry of Education, Science and Technology. This work was also supported by the RFID R&D program of MKE/KEIT [10035225, Development of a Core Technology for High-Performance AMOLED on Plastic].

References

1 G. Li, R. Zhu and Y. Yang, *Nat. Photonics*, 2012, **6**, 155.
2 J.-L. Bredas, J. E. Norton, J. Cornil and V. Coropceanu, *Acc. Chem. Res.*, 2009, **42**, 1691.
3 S. Günes, H. Neugebauer and N. S. Sariciftci, *Chem. Rev.*, 2007, **107**, 1324.
4 J. Gao, L. Dou, W. Chen, C.-C. Chen, X. Guo, J. You, B. Bob, W.-H. Chang, J. Strzalka, C. Wang, G. Li and Y. Yang, *Adv. Energy Mater.*, 2014, **4**, 1300739.
5 K. H. Hendriks, G. H. L. Heingtages, V. S. Gevaerts, M. M. Wienk and R. A. J. Janssen, *Angew. Chem., Int. Ed.*, 2013, **52**, 8341.
6 Y. Dong, X. Hu, C. Duan, P. Liu, S. Liu, L. Lan, D. Chen, L. Ying, S. Su, X. Gong, F. Huang and Y. Cao, *Adv. Mater.*, 2013, **25**, 3683.
7 L. Ye, S. Zhang, W. Zhao, H. Yao and J. Hou, *Chem. Mater.*, 2014, **26**, 3603.
8 J. E. Coughlin, Z. B. Henson, G. C. Welch and G. C. Bazan, *Acc. Chem. Res.*, 2014, **47**, 257.
9 H. Zhou, L. Yang and W. You, *Macromolecules*, 2012, **45**, 607.
10 S. Xiao, H. Zhou and W. You, *Macromolecules*, 2008, **41**, 5688.
11 Y. Li, K. Yao, H.-L. Yip, F.-Z. Ding, Y.-X. Xu, X. Li, Y. Chen and A. K.-Y. Jen, *Adv. Funct. Mater.*, 2014, **24**, 3631.

12 E. H. Jung and W. H. Jo, *Energy Environ. Sci.*, 2014, **7**, 650.
13 I. Osaka, M. Shimawaki, H. Mori, I. Doi, E. Miyazaki, T. Koganezawa and K. Takimiya, *J. Am. Chem. Soc.*, 2012, **134**, 3498.
14 Y. J. Kim, Y.-J. Lee, J.-W. Jang, H. Cha, Y.-H. Kim, S.-K. Kwon and C. E. Park, *J. Polym. Sci., Part A: Polym. Chem.*, 2013, **51**, 4742.
15 H. J. Son, B. Carsten, I. H. Jung and L. Yu, *Energy Environ. Sci.*, 2012, **5**, 8158.
16 Y. Li, *Acc. Chem. Res.*, 2012, **45**, 723.
17 H. Zhou, L. Yang, S. Liu and W. You, *Macromolecules*, 2010, **43**, 10390.
18 B. C. Thompson and J. M. J. Frechet, *Angew. Chem., Int. Ed.*, 2008, **47**, 58.
19 L. Huo, J. Hou, S. Zhang, H.-Y. Chen and Y. Yang, *Angew. Chem., Int. Ed.*, 2010, **49**, 1500.
20 X. Wang, S. Chen, Y. Sun, M. Zhang, Y. Li, X. Li and H. Wang, *Polym. Chem.*, 2011, **2**, 2872.
21 H. Zhou, L. Yang, S. C. Price, K. J. Knight and W. You, *Angew. Chem., Int. Ed.*, 2010, **49**, 7992.
22 S. Zhang, L. Ye, Q. Wang, Z. Li, X. Guo, L. Huo, H. Fan and J. Hou, *J. Phys. Chem. C*, 2013, **117**, 9550.
23 Y. J. Kim, H. N. Kim, M.-C. Hwang, Y.-H. Kim and C. E. Park, *Synth. Met.*, 2014, **198**, 93.
24 Y.-J. Cheng, S.-H. Yang and C.-S. Hsu, *Chem. Rev.*, 2009, **109**, 5868.
25 L. Dou, J. Gao, E. Richard, J. You, C.-C. Chen, K. C. Cha, Y. He, G. Li and Y. Yang, *J. Am. Chem. Soc.*, 2012, **134**, 10071.
26 J. J. Benson-Smith, L. Goris, K. Vandewal, K. Haenen, J. V. Manca, D. Vanderzande, D. D. C. Bradley and J. Nelson, *Adv. Funct. Mater.*, 2007, **17**, 451.
27 P. Dutta, W. Yang, S. H. Eom and S.-H. Lee, *Org. Electron.*, 2012, **13**, 273.
28 L. Fan, R. Cui, X. Guo, D. Qian, B. Qiu, J. Yuan, Y. Li, W. Huang, J. Yang, W. Liu, X. Xu, L. Li and Y. Zou, *J. Mater. Chem. C*, 2014, **2**, 5651.
29 H. Zhou, L. Yang, S. Stoneking and W. You, *ACS Appl. Mater. Interfaces*, 2010, **2**, 1377.
30 P. Shen, H. Bin, X. Chen and Y. Li, *Org. Electron.*, 2013, **14**, 3152.
31 H. Bronstein, M. Hurhangee, E. C. Fregoso, D. Beatrup, Y. W. Soon, Z. Huang, A. Hadipour, P. S. Tuladhar, S. Rossbauer, E.-H. Sohn, S. Shoaee, S. D. Dimitrov, J. M. Frost, R. S. Ashraf, T. Kirchartz, S. E. Watkins, K. Song, T. Anthopoulos, J. Nelson, B. P. Rand, J. R. Durrant and I. McCulloch, *Chem. Mater.*, 2013, **25**, 4239.
32 M. Zhang, X. Guo, W. Ma, S. Zhang, L. Huo, H. Ade and J. Hou, *Adv. Mater.*, 2014, **26**, 2089.
33 Y. J. Kim, K. H. Park, J.-j. Ha, D. S. Chung, Y.-H. Kim and C. E. Park, *Phys. Chem. Chem. Phys.*, 2014, **16**, 19874.
34 Y. Wu, Z. Li, W. Ma, Y. Huang, L. Huo, X. Guo, M. Zhang, H. Ade and J. Hou, *Adv. Mater.*, 2013, **25**, 3449.
35 J. J. Intemann, K. Yao, Y.-X. Li, H.-L. Yip, Y.-X. Xu, P.-W. Liang, C.-C. Chueh, F.-Z. Ding, X. Yang, X. Li, Y. Chen and A. K.-Y. Jen, *Adv. Funct. Mater.*, 2014, **24**, 1465.
36 A. A. B. Alghamdi, D. C. Watters, H. Yi, S. A. Faifi, M. S. Almeataq, D. Coles, J. Kingsley, D. G. Lidzey and A. Iraqi, *J. Mater. Chem. A*, 2013, **1**, 5165.
37 Z. Ma, W. Sun, S. Himmelberger, K. Vandewal, Z. Tang, J. Bergqvist, A. Salleo, J. W. Andreasen, O. Inganas, M. R. Andersson, C. Muller, F. Zhang and E. Wang, *Energy Environ. Sci.*, 2014, **7**, 361.
38 H.-J. Yun, Y.-J. Lee, S. J. Yoo, D. S. Chung, Y.-H. Kim and S.-K. Kwon, *Chem.–Eur. J.*, 2013, **19**, 13242.
39 J. Zhou, X. Wan, Y. Liu, Y. Zuo, Z. Li, G. He, G. Long, W. Ni, C. Li, X. Su and Y. Chen, *J. Am. Chem. Soc.*, 2012, **134**, 16345.
40 J. Jo, A. Pron, P. Berrouard, W. L. Leong, J. D. Yuen, J. S. Moon, M. Leclerc and A. J. Heeger, *Adv. Energy Mater.*, 2012, **2**, 1397.
41 E. Wang, Z. Ma, Z. Zhang, K. Vandewal, P. Henriksson, O. Inganas, F. Zhang and M. R. Andersson, *J. Am. Chem. Soc.*, 2011, **133**, 14244.
42 Y. Deng, J. Liu, J. Wang, L. Liu, W. Li, H. Tian, X. Zhang, Z. Xie, Y. Geng and F. Wang, *Adv. Mater.*, 2014, **26**, 471.
43 H. Hoppe and N. S. Sariciftci, *J. Mater. Res.*, 2004, **19**, 1924.
44 H. Hoppe and N. S. Sariciftci, *J. Mater. Chem.*, 2006, **16**, 45.
45 L. Huo, J. Hou, S. Zhang, G. Y. Chen and Y. Yang, *Angew. Chem., Int. Ed.*, 2010, **49**, 1510.
46 Z. Xiao, J. Subbiah, K. Sun, S. Ji, D. J. Jones, A. B. Holmes and W. W. H. Wong, *J. Mater. Chem. C*, 2014, **2**, 1306.
47 S. H. Park, A. Roy, S. Beaupre, S. Cho, N. Coates, J. S. Moon, D. Moses, M. Leclerc, K. Lee and A. J. Heeger, *Nat. Photonics*, 2009, **3**, 297.
48 D. S. Chung, Y. Rho, M. Ree, S.-K. Kwon and Y.-H. Kim, *ACS Appl. Mater. Interfaces*, 2012, **4**, 4758.
49 R. Noriega, J. Rivnay, K. Vandewal, F. P. V. Koch, N. Stingelin, P. Smith, M. F. Toney and A. Salleo, *Nat. Mater.*, 2013, **12**, 1038.
50 P. Muller-Buschbaum, *Adv. Mater.*, 2014, **26**, 7692.
51 B. Wang, S. W. Tsang, W. Zhang, Y. Tao and M. S. Wong, *Chem. Commun.*, 2011, **47**, 9471.
52 J. E. Carlé, J. W. Andreasen, M. Jørgensen and F. C. Krebs, *Sol. Energy Mater. Sol. Cells*, 2010, **94**, 774.
53 J. E. Carlé, M. Jørgensen and F. C. Krebs, *J. Photonics Energy*, 2011, **1**, 1.

